Incorporation of Mean/Maximum Stress Effects in the Multiaxial Racetrack Filter

Marco Antonio Meggiolaro, Jaime Tupiassú Pinho de Castro
Pontifical Catholic University of Rio de Janeiro, PUC-Rio, R. Marquês de São Vicente 225, Rio de Janeiro, 22451-900, Brazil
meggi@puc-rio.br, jtcastro@puc-rio.br

Hao Wu
School of Aerospace Engineering and Applied Mechanics Tongji University, Siping Road 1239, 200092, Shanghai, P.R.China
wuhao@tongji.edu.cn

ABSTRACT. This work extends the Multiaxial Racetrack Filter (MRF) to incorporate mean or maximum stress effects, adopting a filter amplitude that depends on the current stress level along the stress or strain path. In this way, a small stress or strain amplitude event can be filtered out if associated with a non-damaging low mean or peak stress level, while another event with the very same amplitude can be preserved if happening under a more damaging high mean or peak stress level. The variable value of the filter amplitude must be calculated in real time, thus it cannot depend on the peak or mean stresses along a load event, because it would require cycle identification and as so information about future events. Instead, mean/maximum stress effects are modeled in the filter as a function of the current (instantaneous) hydrostatic or normal stress along the multiaxial load path, respectively for invariant-based and critical-plane models. The MRF efficiency is evaluated from tension-torsion experiments in 316L stainless steel tubular specimens under non-proportional (NP) load paths, showing it can robustly filter out non-damaging events even under multiaxial NP variable amplitude loading histories.

KEYWORDS. Multiaxial racetrack filter; Mean/peak stress effects; Non-damaging events; Multiaxial loads.

Citation: Meggiolaro, M.A., de Castro, J.T.P., Wu, H., Incorporation of Mean/Maximum Stress Effects in the Multiaxial Racetrack Filter, Frattura ed Integrità Strutturale, 38 (2016) 67-75.

Received: 12.05.2016
Accepted: 10.06.2016
Published: 01.10.2016

INTRODUCTION

Unlike frequency filters that clean but distort originally noisy signals, the uniaxial racetrack filter [1, 2] is an efficient and well-proven *amplitude* filter. It can eliminate non-damaging events from uniaxial load histories without changing the original loading order and its overall shape, much improving the efficiency of practical fatigue

damage calculations from unavoidably noisy strain signals measured under actual field conditions. The racetrack generalization to properly filter multiaxial non-proportional (NP) variable amplitude loading (VAL) histories is even more useful for practical applications. In fact, it can allow a dramatic reduction in the intrinsically high computational cost of fatigue damage calculations from multiaxial strain measurements, which besides noisy, usually are oversampled, too long, and/or contain too many non-damaging low-amplitude events that do not affect the damage values, but can much delay their calculation.

However, multiaxial racetrack filter (MRF) procedures are not as simple as the uniaxial ones. Indeed, not even the removal from multiaxial VAL histories of apparently redundant data points that are not reversals of any of their stress or strain components is appropriate because: (i) the path between two load reversals is needed to evaluate the path-equivalent stress or strain associated with each rainflow count, e.g. using a convex-enclosure method [3, 4]; and (ii) reversal points from a multiaxial rainflow algorithm might not occur at a reversal of one of the stress or strain components.

To solve issues like those, a truly MRF that can remove non-damaging events from multiaxial load paths represented in a sub-space from the 6D stress or strain space has been recently proposed in [5], extending its *peg inside a slot* 1D analogy illustrated in Fig. 1 to the 6D stress or strain spaces. Its specifiable filter amplitude defines the radius of a hyper-sphere (or a sphere in 3D or a circle in 2D load histories, respectively), which translates along the load path while filtering out any small load oscillations happening within its interior region. The basic MRF procedures are briefly outlined in Fig. 2. Further details on the basic MRF procedures can be found in [5, 6].

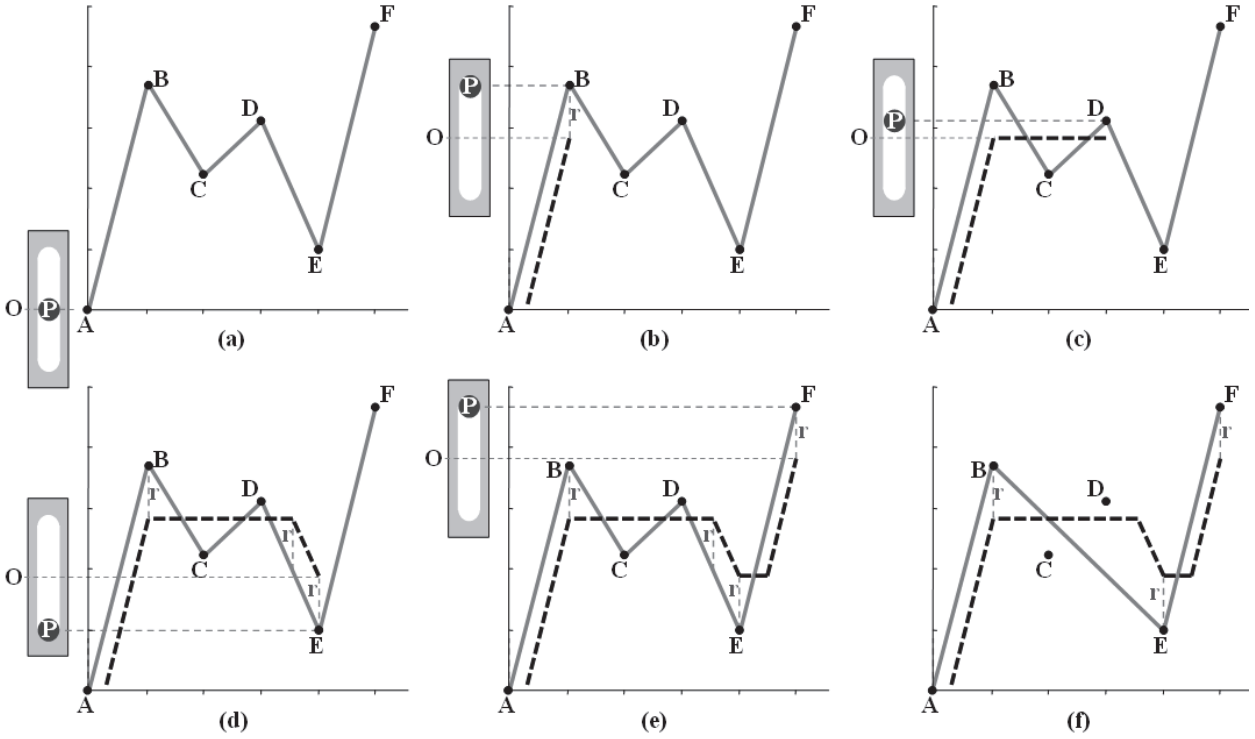

Figure 1: Analogy between the uniaxial racetrack filter and a peg P oscillating inside a slotted plate with center O and slot range 2r. The peg oscillates following the original history, resulting in translations of O represented by the dashed line.

The use of a 5D deviatoric stress or strain space allows the MRF to be applied to invariant-based damage models, which assume fatigue damage is controlled by invariants like the von Mises ranges and hydrostatic stresses, such as in Crossland's pioneer model [7]. For a given stress history, this 5D space is represented by the deviatoric vector

$$\vec{s}' \equiv \left[\sigma_x - (\sigma_y + \sigma_z)/2 \quad (\sigma_y - \sigma_z)\sqrt{3}/2 \quad \tau_{xy}\sqrt{3} \quad \tau_{xz}\sqrt{3} \quad \tau_{yz}\sqrt{3} \right]^T \tag{1}$$

Since the norm of $\vec{s}'$ is equal to the von Mises stress, all distances and filter amplitudes in this 5D sub-space have a physical meaning, they are the von Mises range or the relative von Mises stresses $\Delta\sigma_{Mises}$ for a straight path between two stress states. Alternatively, for a given strain history, the 5D space is defined by the deviatoric vector

$$\vec{e}' \equiv \left[\varepsilon_x - (\varepsilon_y + \varepsilon_z)/2 \quad (\varepsilon_y - \varepsilon_z)\sqrt{3}/2 \quad \gamma_{xy}\sqrt{3}/2 \quad \gamma_{xz}\sqrt{3}/2 \quad \gamma_{yz}\sqrt{3}/2 \right]^T \tag{2}$$

A sixth dimension could also be considered in the above 5D spaces, which would store the hydrostatic stress σ_h or strain ε_h of the current state, allowing the filtering of not only deviatoric components, but also of their hydrostatic components. For 2D tension-torsion histories with stress paths defined by the normal and shear components σ_x and τ_{xy}, it is found that $\sigma_y = \sigma_z = \tau_{xz} = \tau_{yz} = 0$, while $\varepsilon_y = \varepsilon_z = -\bar{\nu} \cdot \varepsilon_x$ and $\gamma_{xz} = \gamma_{yz} = 0$, where $\bar{\nu}$ is an effective Poisson ratio. In this case,

$$\vec{s}' \equiv \left[\sigma_x \quad 0 \quad \tau_{xy}\sqrt{3} \quad 0 \quad 0 \right]^T \text{ and } \vec{e}' \equiv \left[\varepsilon_x \cdot (1+\bar{\nu}) \quad 0 \quad \gamma_{xy}\sqrt{3}/2 \quad 0 \quad 0 \right]^T \tag{3}$$

therefore the stress or strain paths of such tension-torsion histories can be represented in the 2D deviatoric diagrams $\sigma_x \times \tau_{xy}\sqrt{3}$ or $\varepsilon_x \cdot (1+\bar{\nu}) \times \gamma_{xy}\sqrt{3}/2$, which are sub-spaces from the 5D deviatoric spaces from Eq. (3).

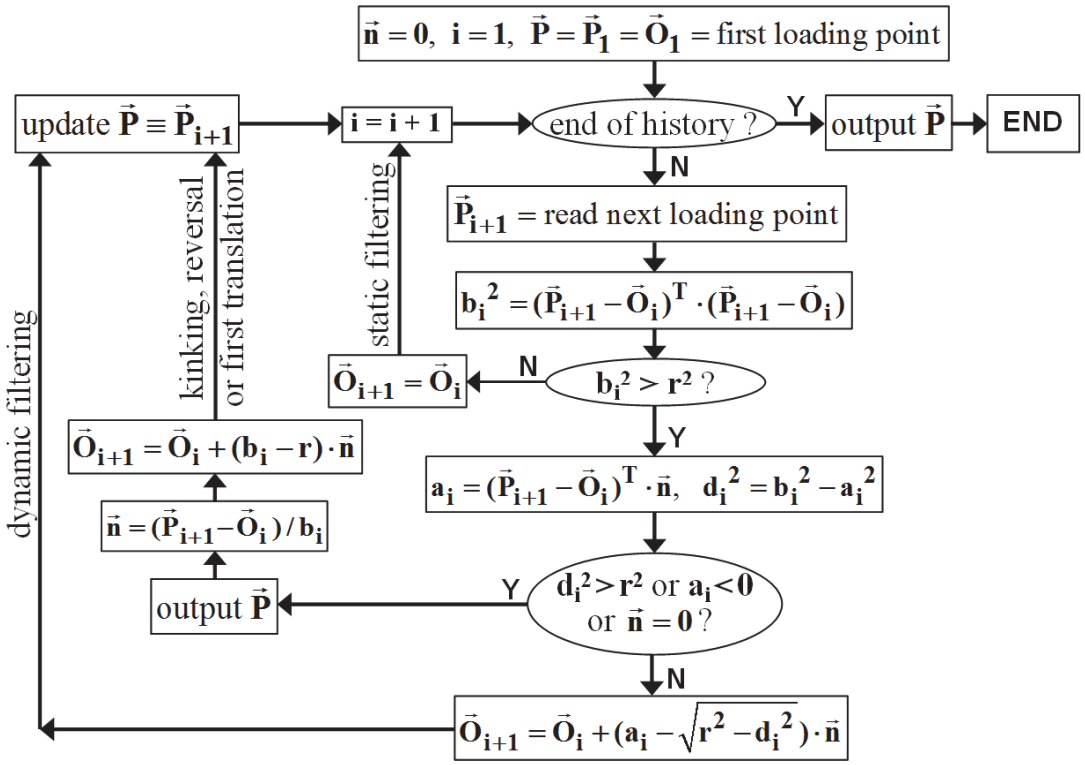

Figure 2: Multiaxial racetrack algorithm, with the filtered history resulting from the $\vec{P}$ output values, where $\vec{n}$ is the hyper-sphere translation direction and $\vec{O}_i$ its center during each loading event *i*.

Fig. 3 shows an idealized tension-torsion history represented in the $\sigma_x \times \tau_{xy}\sqrt{3}$ normal-effective shear stress diagram, with the original path points represented as × markers. For a filter amplitude *r = 80MPa* (the radius of the circle shown in the figure centered at the end of the history, assuming it represents well the fatigue damage threshold), the MRF results in a much reduced number of points, represented with square and triangular markers. Note in this figure that many points from such oversampled example are filtered out. Note as well that small and supposedly non-damaging normal stress or effective shear stress oscillations are also filtered out, as seen in the upper part of the figure. The original *1,315* data points of this idealized history are dramatically reduced to only *56*, significantly reducing the computational cost of subsequent multiaxial rainflow or fatigue damage calculations, without affecting their results if the filter amplitude is well chosen. This simple example should be enough to justify the claim that the MRF is a much useful tool for practical fatigue damage calculations. In fact, its major drawback, the proper specification of the value of the filter amplitude, is not a major issue

when using the MRF. It is in fact similar to the problem of finding a properly refined mesh for finite element calculations, which in practice can be found by sequentially refining it until the calculations converge.

The MRF can also be used for projected histories on a candidate plane, to reduce computational costs in multiaxial fatigue damage calculations based on critical-plane approaches [2-4, 8]. For shear-based models, the 2D spaces $[\tau_A\ \tau_B]^T$ or $[\gamma_A\ \gamma_B]^T$ could be adopted in the MRF, where the subscripts A and B represent the in-plane and out-of-plane shear directions of a candidate plane. For tensile-based damage models, the traditional uniaxial racetrack filter could be applied to the 1D spaces $[\sigma_\perp]$ or $[\varepsilon_\perp]$, where $\sigma_\perp$ and $\varepsilon_\perp$ are the normal stress and strain perpendicular to the candidate plane. Alternatively, for multiaxial models that mix both shear and tensile damage, the 3D stress or strain spaces $[\tau_A\ \tau_B\ \sigma_\perp]^T$ or $[\gamma_A\ \gamma_B\ \varepsilon_\perp]^T$ could be used instead in the MRF.

However, the original MRF uses fixed filter amplitudes, not a good choice for load histories that contain significant mean load variations due to the asymmetric fatigue damage behavior, which is much more sensitive to tensile mean loads. The purpose of this work is to properly solve this issue.

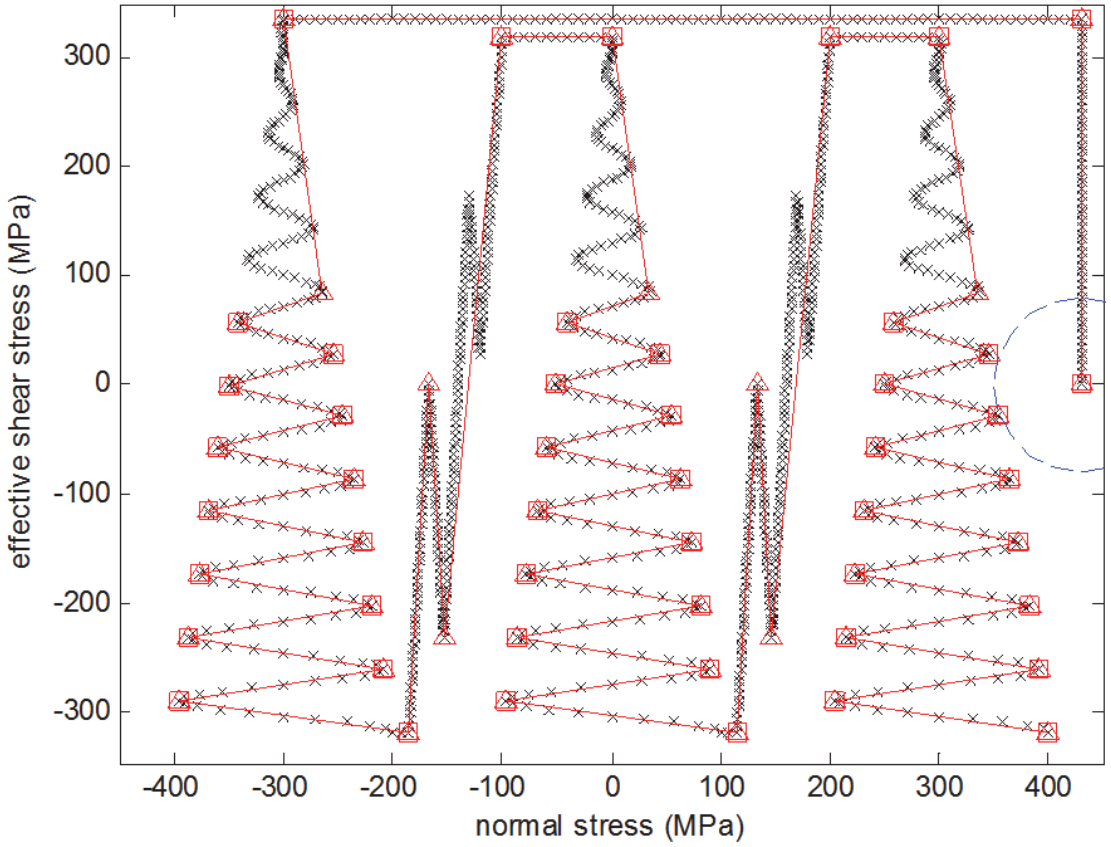

Figure 3: Original points from an idealized $\sigma_x \times \tau_{xy}\sqrt{3}$ stress path (× markers), and outputs from the MRF (square and triangular markers) for a filter amplitude $r = 80MPa$.

MRF With Mean/Maximum Stress Effects

As mentioned above, the original implementation of the MRF [5-6] uses a fixed filter amplitude r. However, since tensile load histories tend to be more damaging due to mean/maximum stress effects in multiaxial fatigue, they would benefit from a choice of lower values of r, to avoid filtering out damaging events. On the other hand, compressive histories could allow the choice of higher filter amplitudes, filtering out more points without compromising the damage calculations.

Such an improved MRF, optimized to consider mean/maximum stress effects on fatigue damage, can be implemented adopting a filter amplitude r that depends on the current stress level. In this way, a small stress or strain amplitude event

could be filtered out if associated with a non-damaging low peak-stress level, while another event with the same amplitude could be preserved if happening under a damaging high peak-stress level.
However, this is easier said than done. The filter amplitude must be calculated in real time (or else it would lose efficiency), so it cannot be a function of the peak or mean stresses along a load event, which would require cycle identification and information about future events. Instead, mean/maximum-stress effects are modeled in the filter in a simplified way, as a function of the current (instantaneous) hydrostatic σ_h or normal $\sigma_\perp$ stress along the load path, respectively for invariant-based and critical-plane models, as briefly outlined in [6]. Crossland's invariant-based model [7], e.g., adopts an infinite-life criterion

$$\Delta\tau_{Mises}/2 + \alpha_C \cdot (3\cdot\sigma_{h\max}) = \beta_C \tag{4}$$

where $\Delta\tau_{Mises}$ is a path-equivalent von Mises shear stress range, σ_{hmax} is the peak hydrostatic component, and α_C and β_C are material constants. If this damage model is adopted, then the stress history could be represented in the previously defined 5D deviatoric space $\vec{s}'$, assuming a σ_h-dependent variable filter amplitude

$$r \equiv \Delta\sigma_{Mises}/2 = \Delta\tau_{Mises}\sqrt{3}/2 = (\beta_C\sqrt{3}) - (3\sqrt{3}\alpha_C)\cdot\sigma_h \tag{5}$$

On the other hand, Findley's critical-plane model [9] assumes that

$$\Delta\tau/2 + \alpha_F\cdot\sigma_{\perp\max} = \beta_F \tag{6}$$

where $\Delta\tau$ and $\sigma_{\perp max}$ are the shear stress range and peak normal stress on the critical plane, and α_F and β_F are material constants. Using this damage model, the shear stress history on the considered candidate plane could be represented in the 2D shear stress space $[\tau_A\ \tau_B]^T$, while adopting a $\sigma_\perp$-dependent variable filter amplitude

$$r \equiv \Delta\tau/2 = \beta_F - \alpha_F\cdot\sigma_{\perp\max} \tag{7}$$

Fatemi-Socie's critical-plane model [10] assumes that

$$\frac{\Delta\gamma}{2}\cdot\left(1+\alpha_{FS}\frac{\sigma_{\perp\max}}{S_{Yc}}\right) = \frac{\tau_c}{G}(2N)^{b_\gamma} + \gamma_c(2N)^{c_\gamma} \tag{8}$$

where $\Delta\gamma$ and $\sigma_{\perp max}$ are the shear strain range and peak normal stress on the critical plane, N is the associated fatigue life in cycles, G and S_{Yc} are the material's shear modulus and cyclic yield strength, and α_{FS}, τ_c, γ_c, b_γ and c_γ are material constants. For this damage model, the shear strain history on the considered candidate plane could be represented in the 2D shear strain space $[\gamma_A\ \gamma_B]^T$, while adopting a $\sigma_\perp$-dependent variable filter amplitude

$$r \equiv \frac{\Delta\gamma}{2} = \left(\frac{\tau_c}{G}(2N_L)^{b_\gamma} + \gamma_c(2N_L)^{c_\gamma}\right) \Big/ \left(1+\alpha_{FS}\frac{\sigma_\perp}{S_{Yc}}\right) \tag{9}$$

where N_L is the number of cycles associated with the stress-life fatigue limit, or any other user-defined fatigue life level.
A high-cycle variation of the above variable filter amplitude can also be defined, based on a shear stress instead of shear strain amplitude, giving

$$r = \tau_L \Big/ \left(1+\alpha_U\cdot\sigma_\perp/S_U\right) \tag{10}$$

where τ_L is the shear fatigue limit under zero mean stresses, α_U is a material constant and S_U is its ultimate strength.
In all above cases for Crossland's, Findley's and Fatemi-Socie's models or its variations, the filter amplitude r becomes instantaneously smaller for higher σ_h or $\sigma_\perp$ stress levels, to avoid filtering out damaging events. Analogously, similar expressions for such a variable r could be easily derived for other multiaxial fatigue damage models.

These ideas have been implemented in a suitable computer code and used to analyze the results obtained from two challenging tests that involved non-proportional tension-torsion load histories applied on tubular specimens, as well as another idealized bi-axial load history that illustrates well the effects of high mean loads, as discussed next.

EXPERIMENTAL RESULTS

The improved version of the MRF, proposed in this work to properly consider the difference between the well-known effects caused by tensile and compressive mean loads on fatigue damage, is evaluated using experimental and idealized tension-torsion 2D stress histories. The experiments are performed on annealed tubular 316L stainless steel specimens in a multiaxial servo-hydraulic testing machine. The cyclic properties of this 316L steel are obtained from simple uniaxial tests, using standard procedures. Its Ramberg-Osgood uniaxial cyclic hardening coefficient and exponent are 874MPa and 0.123, with Young's modulus 193GPa and Poisson ratio 0.3. This material has been chosen for those tests because it presents a significant non-proportional (NP) hardening effect as well, which cannot be neglected in multiaxial fatigue damage calculations, as discussed below.

The two experiments reported below consist of strain-controlled tension-torsion cycles applied to identical tubular specimens, one for the cross and one for the x-shaped paths from Fig. 2, represented in the normal-effective shear strain space $\varepsilon_x \times \gamma_{xy}/\sqrt{3}$.

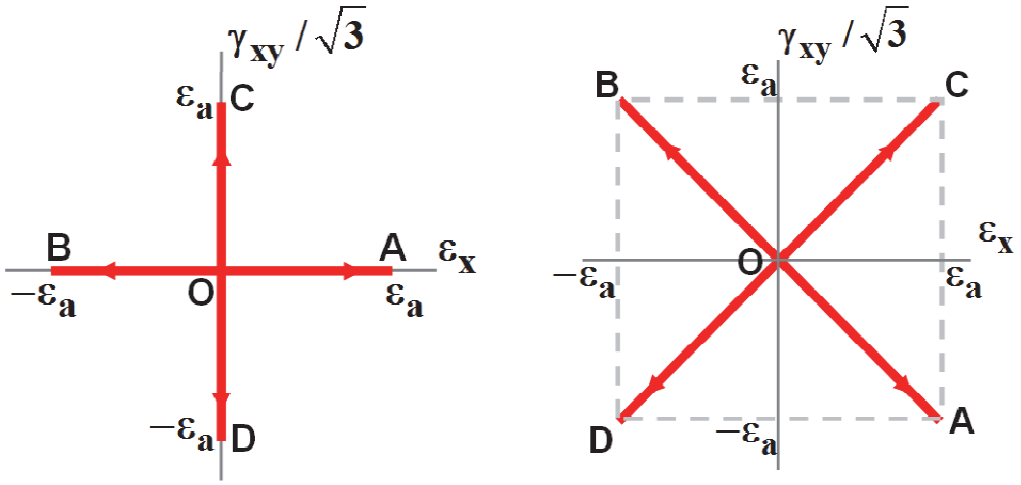

Figure 2: Applied $\varepsilon_x \times \gamma_{xy}/\sqrt{3}$ strain paths on two tension-torsion tubular specimens, with successively imposed amplitudes ε_a = *0.2%*, *0.4%*, *0.6%* and *0.8%* in each case.

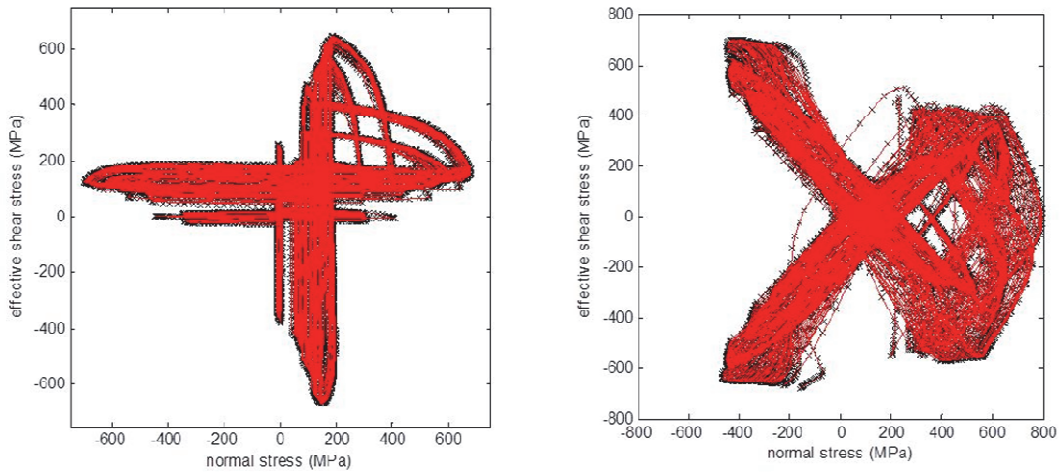

Figure 3: Experimentally measured data points (× markers) from the $\sigma_x \times \tau_{xy}\sqrt{3}$ stress paths induced by the cross and x-shaped inputs from Fig. 2, and associated outputs from the MRF (solid lines) for a chosen filter amplitude r = *7MPa*.

For each specimen, several load periods are applied for a given normal strain amplitude ε_a = *0.2%*, *0.4%*, *0.6%* and *0.8%*. The resulting normal-effective shear stress paths $\sigma_x \times \tau_{xy}\sqrt{3}$ are very complex, involving high NP hardening effects and transients, see Fig. 3.

Fig. 3 shows the experimentally measured data points (× markers) from each of the two specimens, as well as the MRF output (solid lines) for a filter amplitude r = *7MPa*. For the cross-shaped path, 95% of the measured points were filtered out, while for the x-shaped case 87% were eliminated, significantly reducing the computational costs of subsequent fatigue life calculations. Notice that, despite being highly filtered, the MRF outputs can almost exactly describe the original history, capturing not only all reversal points but also the path shape, which is a most important feature for equivalent-range multiaxial fatigue damage calculations.

Fig. 4 shows a random single period of each of the Fig. 3 paths, where the square markers represent the MRF output, filtering out most of the original stress points.

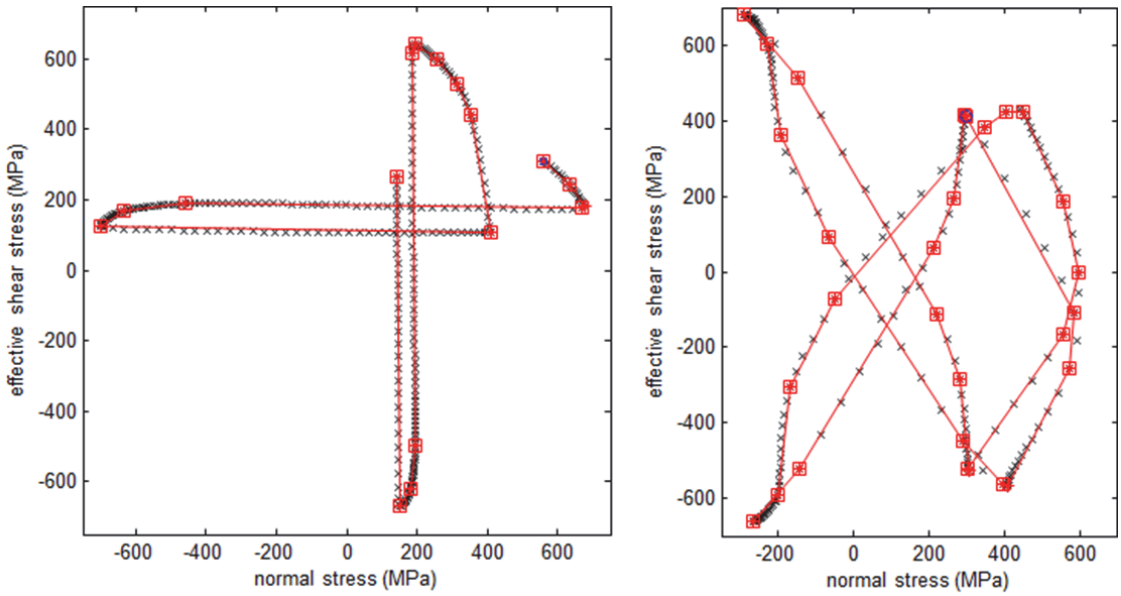

Figure 4: Experimentally measured data points (× markers) for a single period of the cross and x-shaped histories, and associated outputs from the MRF (square markers) for a filter amplitude r = *7MPa*.

To better evaluate the mean/maximum stress effects in the proposed modification of the MRF, the idealized tension-torsion stress history from Fig. 1 is now filtered according to a filter amplitude based e.g. on Fatemi-Socie's model, shown in Eqs. (9) and (10) respectively for strain or stress histories. Fig. 5 plots the idealized tension-torsion stress history in a normal-effective shear stress diagram, with the original path points represented as × markers.

Assuming Fig. 5 represents the $\sigma_\perp \times \tau_A\sqrt{3}$ history of the normal stress and in-plane shear stress components on a candidate plane, the variable filter amplitude from Eq. (10) could be used, but multiplied by $\sqrt{3}$ (due to the scaling from τ_A to $\tau_A\sqrt{3}$) to give

$$r = \tau_L\sqrt{3} \Big/ \left(1+\alpha_U \cdot \sigma_\perp / S_U\right) \tag{11}$$

For a hypothetical component with $\tau_L\sqrt{3} = 80MPa$, S_U = *515MPa*, and α_U = *0.66*, the above variable filter amplitude becomes $r = 80 \Big/ \left(1+0.66\cdot\sigma_\perp/515\right)$. Fig. 5 shows the MRF output adopting such a variable r, where the remaining (unfiltered) points are marked as squares or triangles. Notice how most of the normal oscillations were filtered out under a −300MPa compressive mean normal stress, while very few of them were filtered under +300MPa. And the small shear cycle near the −120MPa compressive normal stress was filtered out, while the same shear cycle at +180MPa was not, a desirable behavior for an amplitude filter that considers mean/maximum stress effects.

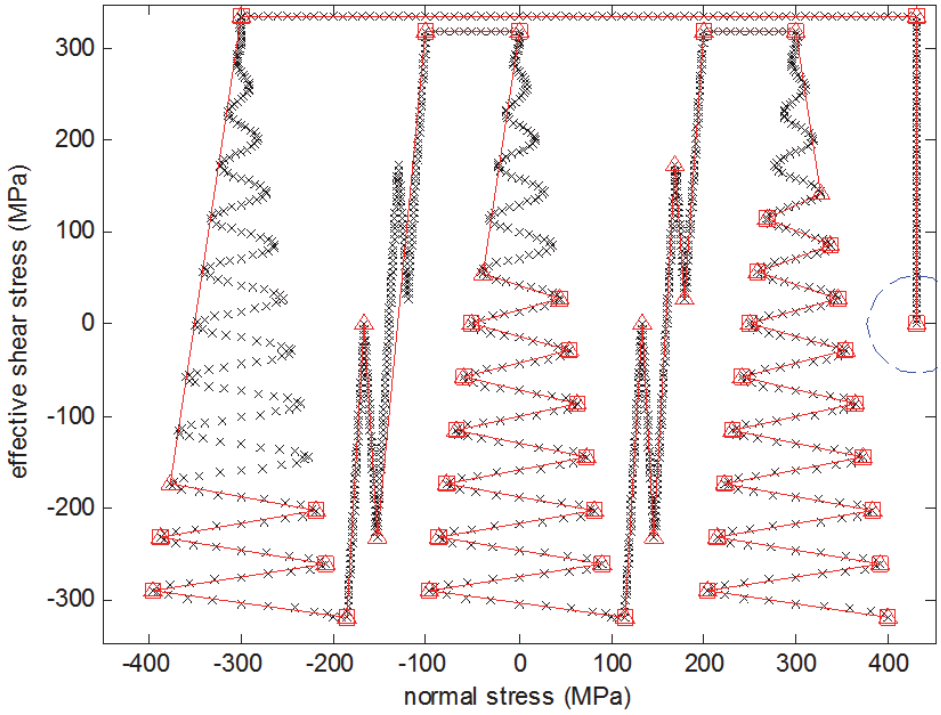

Figure 5: Original points from an idealized $\sigma_{\perp} \times \tau_A \sqrt{3}$ stress path (× markers), and outputs from the MRF (square and triangular markers), considering mean stress effects.

CONCLUSIONS

The Multiaxial Racetrack Filter (MRF) is an efficient amplitude filter applicable to multiaxial histories and fatigue damage models based on invariants or on the critical-plane approach. The MRF is able to filter out low-amplitude events, significantly decreasing the computational cost of subsequent multiaxial fatigue-damage calculations. In this work, mean/maximum stress effects were incorporated into the MRF. The proposed variable filter amplitudes allowed the algorithm to efficiently filter out events based on their damage parameter. In this way, lower filter amplitudes are automatically used for tensile histories, and higher filter amplitudes for compressive ones, optimizing the filter efficiency without neglecting significant damaging events.

REFERENCES

[1] Fuchs, H.O., Nelson, D.V., Burke, M.A., Toomay, T.L., Shortcuts in Cumulative Damage Analysis, SAE Automobile Engineering Meeting Paper 730565 (1973).

[2] Castro, J.T.P., Meggiolaro, M.A., Fatigue Design Techniques (in 3 volumes), CreateSpace, Scotts Valley, CA, USA (2016).

[3] Meggiolaro, M.A., Castro, J.T.P., An improved multiaxial rainflow algorithm for non-proportional stress or strain histories - part I: enclosing surface methods, Int. J. Fatigue, 42 (2012) 217-226. doi:10.1016/j.ijfatigue.2011.10.014

[4] Meggiolaro, M.A., Castro, J.T.P., Wu, H., Invariant-based and critical-plane rainflow approaches for fatigue life prediction under multiaxial variable amplitude loading, Procedia Engineering, 101 (2015) 69-76. doi: 10.1016/j.proeng.2015.02.010

[5] Meggiolaro, M.A., Castro, J.T.P., Wu, H., Shortcuts in multiple dimensions: the multiaxial racetrack filter, Frattura ed Integrità Strutturale, 33 (2015) 368-375. doi: 10.3221/IGF-ESIS.33.40

[6] Wu, H., Meggiolaro, M.A., Castro, J.T.P., Validation of the multiaxial racetrack amplitude filter, Int. J. Fatigue, 87 (2016) 167-179. doi: 10.1016/j.ijfatigue.2016.01.016

[7] Crossland, B., Effect of large hydrostatic pressures on the torsional fatigue strength of an alloy steel. Int. Conf. on Fatigue of Metals, London: IMechE (1956) 138-149.
[8] Bannantine, J.A., Socie, D.F., A variable amplitude multiaxial fatigue life prediction method, in Fatigue under Biaxial and Multiaxial Loading, ESIS, 10 (1991) 35-51.
[9] Findley, W.N., A theory for the effect of mean stress on fatigue of metals under combined torsion and axial load or bending, J. Eng. Industry, 81 (1959) 301-306.
[10] Fatemi, A., Socie, D.F., A critical plane approach to multiaxial damage including out-of-phase loading, Fatigue Fract. Eng. Mater. Struct., 11 (1988) 149-166.